NOTES AND CORRESPONDENCE

Evaluation of a UHF Radar Surface Current Mapping System in an Intertidal Salt Marsh

RICHARD STYLES

Marine Science Program, and Department of Geological Sciences, University of South Carolina, Columbia, South Carolina

CALVIN C. TEAGUE

CODAR Ocean Sensors, Ltd., Mountain View, California

(Manuscript received 26 October 2006, in final form 5 February 2007)

ABSTRACT

A UHF RiverSonde radar system was deployed in an intertidal salt marsh during November and December 2005 near Georgetown, South Carolina. The purpose of this experiment was to evaluate radar performance in a coastal plain salt marsh, where the channels are highly sinuous and the flow is dominated by tides. To help evaluate radar performance, an acoustic current profiler was placed in a large subtidal channel located in the field of view of the radar. Comparisons indicated that the radar accurately reproduced both the magnitude and phasing of the surface current. Spatial coverage was generally good in the channels but much more sporadic over the marsh platform. Temporal coverage in the channel was also good and correlated with wind speed. Reliable measurements were obtained under wind speeds as low as 2–3 m s^{-1}, which are common at this site. In addition, some unexpected signals were seen at near zero Doppler shift, which were attributed to the saltwater vegetation *Spartina alterniflora*, which acted as effective radar targets. However, these signals were uncorrelated and likely can be filtered.

1. Introduction

Over the last decade, the application of microwave radar technology to measure surface currents and discharge in fluvial systems has grown substantially (e.g., Costa et al. 2000, 2006; Teague et al. 2001, 2005; Melcher et al. 2002; Plant et al. 2005; Spain et al. 2006). Radars measure surface currents on the principle of Bragg scattering off the roughness of the water surface (Barrick et al. 1977). Typically, an antenna array is placed near the shoreline and transmits a radial signal that is reflected by surface gravity waves that have a wavelength of one-half of the radio wavelength and that are traveling radially toward or away from the radar. The return signal is Doppler shifted above and below the transmitted frequency by an amount proportional to the phase velocity of the waves. If the waves are propagating on a current, the return signal is Doppler shifted by an additional amount. The amount of the additional frequency shift is directly proportional to current speed, providing accurate speed measurements along radial lines converging on the antenna. To compute total surface vectors, a pair of radar installations is displaced laterally along a shoreline. The radial vectors in the overlap region are combined to produce the total surface vector velocity. Because the radio signal is transmitted in a broad angular swath, current measurements are acquired simultaneously at many locations across the water surface.

Intertidal salt marshes, which are common to many coastal regions throughout the world, provide an intriguing setting to apply ultrahigh-frequency (UHF) radar technology. Topographically, salt marshes consist of an extensive cover of relatively featureless marsh platforms dissected by a network of highly sinuous sub- and intertidal channels. The flow is tidal and is accompanied by large, rhythmic fluctuations in water depth

Corresponding author address: Richard Styles, Marine Science Program, and Department of Geological Sciences, University of South Carolina, Columbia, SC 29208.
E-mail: rstyles@geol.sc.edu

DOI: 10.1175/2007JTECHO538.1

such that the marsh and intertidal creeks drain and fill with each tidal cycle. The marsh platform is covered by a thick canopy of vegetation. One of the more common types found along the southeast coast of the United States is *Spartina alterniflora*. *Spartina* forms a thick canopy over the marsh platform but is absent from the creeks and channels, which are lower in elevation. Determining flow paths on a scale large enough to assess spatial gradients in salt marshes is impractical to the point of impossibility using traditional single point or profiling current measuring technology. Within the marsh canopy, current meters are intrusive and the vegetation surrounding the instruments usually is removed or damaged during the deployment setup. To resolve the flow would require an extensive array of current meters, which interfere with the natural state of the landscape, and therefore artificially alter flow patterns. UHF radar represents a promising alternative to measuring spatial flow patterns on a scale sufficient to quantify the hydrodynamic regime of intertidal salt marshes, yet ensures a nonintrusive approach.

As far as the authors are aware, this note describes the first application of UHF radar technology to an intertidal salt marsh. The purpose of this note is to gauge the temporal and spatial effectiveness of UHF radar technology in this topographically complex and densely vegetated environment. The next section describes a field experiment in which we installed a single RiverSonde UHF system (Teague et al. 2003) in an intertidal salt marsh located near Georgetown, South Carolina. This is followed by preliminary results, which provide a measure of the effectiveness and feasibility of using this technology in marshes. On the basis of the results, the discussion briefly describes some potential future technical considerations that should be addressed to further explore applications of UHF radars in intertidal salt marshes.

2. Methods

In November 2005, we deployed a 340-MHz UHF RiverSonde radar in the North Inlet-Winyah Bay National Estuarine Research Reserve located near Georgetown, South Carolina (Fig. 1). The RiverSonde system (Teague et al. 2001, 2003) extends the SeaSonde technology to the UHF range with a radar wavelength of 0.88 m. The Bragg-resonant water wavelength is 0.44 m, and gravity waves of that wavelength have a deep-water phase velocity of 0.83 m s^{-1}, resulting in a Doppler shift of 1.88 Hz in the absence of a current. The radar scattering mechanism at this frequency is still predominately first order, as can be seen in the spectra of Fig. 2, obtained under two different wind conditions. The frequency of the Bragg echo in the absence of a current is indicated by the short vertical lines, and the broadening and displacement of the Bragg lines due to the current viewed from different aspect angles are clearly evident. In place of the crossed loops and monopole of the SeaSonde, the RiverSonde antenna consists of three short Yagi antennas displaced from each other by half a radar wavelength with the outer antennas canted away from the central antenna (Teague et al. 2003). The range resolution of the radar was set to 10 m, and Multiple Signal Classification (MUSIC) direction finding (Schmidt 1986) applied to the signals at each frequency bin yielded direction estimates to 1° resolution. The field of view along a radial path was 300 m and encompassed a 180° lateral swath. The antenna was placed at the end of a boardwalk equipped with power to run the system. Two-way communication via a wireless Internet link was established and was useful in downloading data during the deployment and monitoring instrument performance. The antenna was oriented so that the field of view included a large subtidal channel, several intertidal creeks, and an area of salt marsh platform. The antenna and electronics are all contained on a single fiberglass pole (Fig. 1) that is approximately 3 m in length and 0.10 m in diameter. This compact arrangement has the advantage in that the hardware footprint is very small and, therefore, the radar does not significantly disturb the natural environment.

The subtidal channels are the deepest and widest of the three environments and always contain water even at low tide. Because this is the main conduit for tidal exchange between the ocean and marsh surface in North Inlet, flow speeds are typically on the order of tens of centimeters per second (Traynum and Styles 2007). The intertidal creeks are shallower and, like the marsh platform, always drain during each low tide. Maximum flow speeds in these smaller shorter creeks are typically between 10 and 15 cm s^{-1} (Torres and Styles 2007). The marsh platform possesses an extensive cover of *Spartina alterniflora*, a very common type of marine vegetation in the southeastern United States (Leonard and Luther 1995). Because of the dense vegetation, which severely restricts the flow, maximum speeds here are on the order of a few centimeters per second (Voulgaris and Myers 2004; Torres and Styles 2007). Therefore, we have coverage over three distinct areas with very different flow, morphological, and vegetative characteristics.

To independently evaluate radar performance, a Nortek aquadopp current profiler was placed in the sampling range of the antenna. The aquadopp was deployed in the deep subtidal channel east of the antenna,

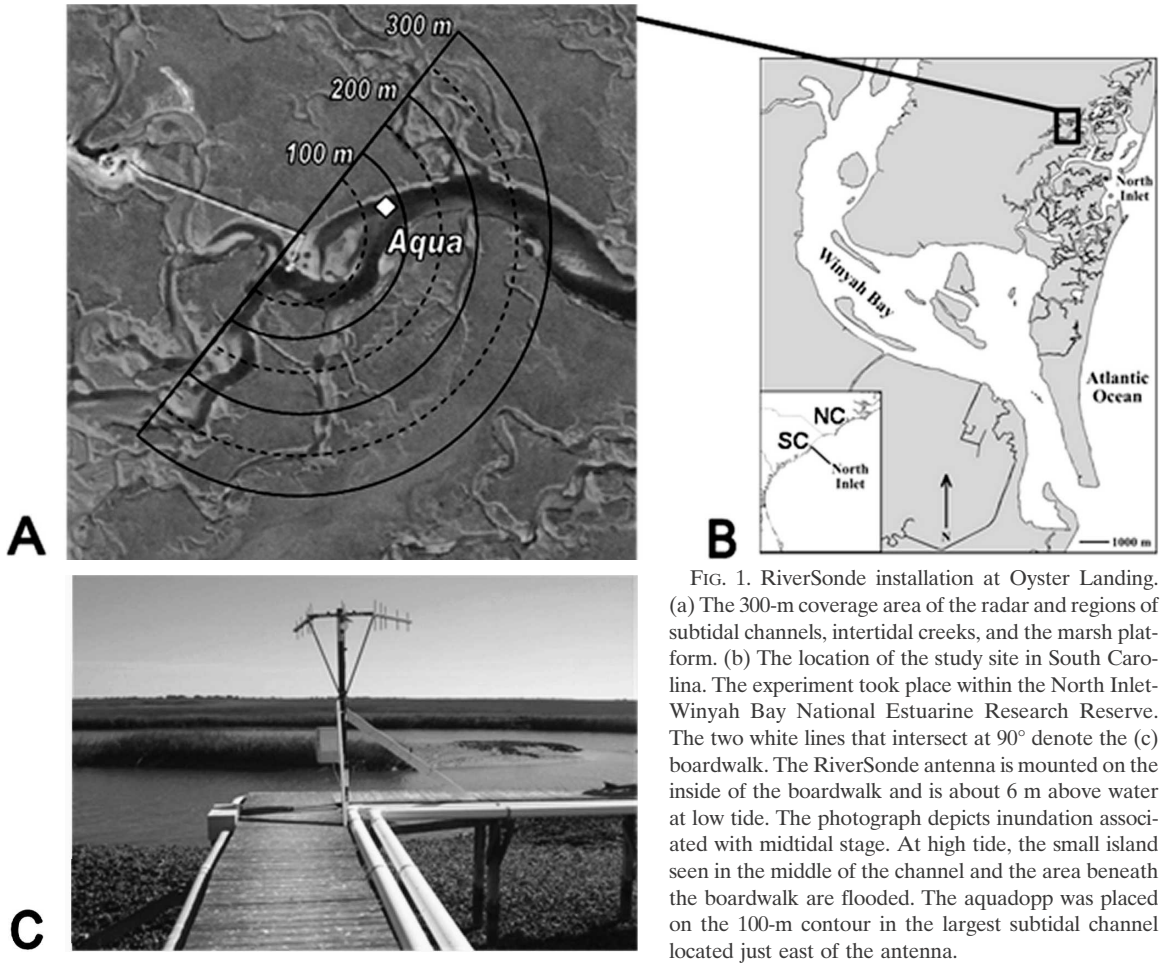

FIG. 1. RiverSonde installation at Oyster Landing. (a) The 300-m coverage area of the radar and regions of subtidal channels, intertidal creeks, and the marsh platform. (b) The location of the study site in South Carolina. The experiment took place within the North Inlet-Winyah Bay National Estuarine Research Reserve. The two white lines that intersect at 90° denote the (c) boardwalk. The RiverSonde antenna is mounted on the inside of the boardwalk and is about 6 m above water at low tide. The photograph depicts inundation associated with midtidal stage. At high tide, the small island seen in the middle of the channel and the area beneath the boardwalk are flooded. The aquadopp was placed on the 100-m contour in the largest subtidal channel located just east of the antenna.

directly in the path of the radar (Fig. 1). The aquadopp was programmed to measure full–water column currents every 10 min, allowing us to compare the radar surface currents to the surface bin of the profiler. The aquadopp sampled a 2-min burst (1-Hz sampling frequency) with a 0.5-m vertical spacing between adjacent bins. Because the water surface fluctuated with the tide, the profiler bin closest to the surface had to be adjusted. This was accomplished by defining the first bin below the water surface, as measured by the aquadopp's pressure transducer, as the bin used in comparisons to the radar. Even at low tide, there was always a submerged bin, so there was no discontinuity in the time series. The profiler was deployed for a 1-week period beginning on 30 November. Logistical constraints and commitments to other filed programs prohibited us from deploying the profiler for the entire experiment. Even so, the results will show that radar coverage during this week was sufficient for a quantitative comparison. Water surface elevation and wind speed and direction were measured at the National Oceanic and Atmospheric Administration (NOAA) Oyster Landing coastal station (ID 8662245) located at the end of the boardwalk. This provided us with wind and water level data within 20 m of the antenna location.

3. Results

a. RiverSonde coverage

Figures 3 and 4 show examples of the radar coverage that is possible during the experiment. The main tidal channels and creeks are outlined in the figure, along with radial vectors obtained over a 12-h period on 16 December 2005. The time begins at midnight (UTC) just before high tide and progresses hourly for almost a full tidal cycle. Because we have only one antenna, all current vectors are oriented along radial lines that emanate from the RiverSonde location. While it is not possible to fully resolve the 2D surface current, the UHF radar provides accurate estimates of the along-channel flow in sections where the channel axis is parallel to the radial component. The RiverSonde was programmed to

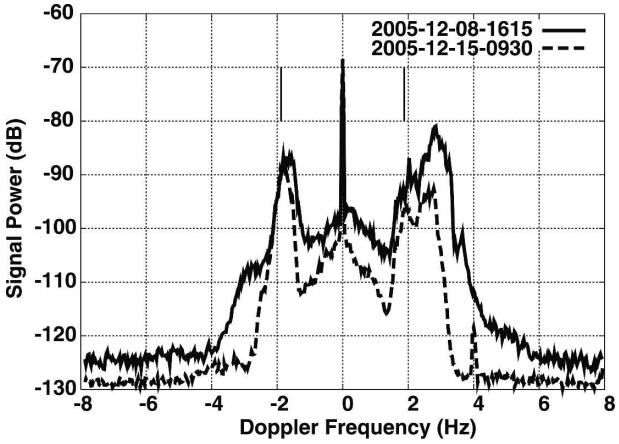

FIG. 2. Power spectra observed under different wind conditions. The solid curve was obtained at 1615 UTC 8 Dec 2005, with a wind speed of 10.1 m s^{-1}. The dashed curve was obtained at 0930 UTC 15 Dec 2005, with a wind speed of 3.7 m s^{-1}. The thin vertical lines near ±2 Hz indicate the positions of the Bragg lines for zero surface current. The noise level between −4 and 5 Hz is 10–15 dB higher for the solid curve.

sample every 1.5 min. These samples were in turn averaged into 15-min intervals to construct time series of radial vectors. Radial vectors are shown only if they were present in at least one-third of the individual 1.5-min observations in the 15-min window and if the standard deviation of those vector magnitudes was less than 10 cm s^{-1}. This simple filtering algorithm proved to be quite effective at eliminating signals near dc between the normal Bragg lines, which apparently are due to reflections by the marsh grass, some of which is visible in Fig. 1. The degree of spatial coverage varies significantly over the 12-h period. Regions noted for having the most coverage include the main subtidal channel located in the right half of each plot. The ocean is located to the east, so the portion of the channel that terminates on the right side of the figure denotes the direction of ebb. A smaller subtidal channel is located southwest of the antenna and is oriented at a small acute angle to the short section of the boardwalk. Ebb currents in this channel will flow toward the array, or generally from south to north.

The first six plots (Fig. 3) progress through time and cover almost a full ebb cycle. The first plot is just before high tide and current vectors in the channels are oriented in the direction of flood. The greatest spatial coverage is seen in the section of the subtidal channel just east of the radar. The second and third plots are around high tide and the vector coverage decreases substantially, as would be expected as the tide is turning and velocities are at a minimum. The remaining plots (4, 5, and 6) show increasing ebb flow and increasing spatial coverage especially in the large subtidal channel east of the radar. The fourth and sixth plots indicate that radar coverage in the main subtidal channel easily extends to the maximum range of the system (300 m) and that the spatial resolution in this channel is very good even around the bend. Note that the maximum range is set prior to the deployment and can be adjusted to either increase or decrease the range. The coverage over the marsh surface is greatly reduced compared to the main channel. However, there appears to be partial sporadic coverage over this time interval.

Figure 4 depicts radar coverage for the remainder of the tidal cycle. The first plot is just before low tide and the vectors still indicate ebbing flow. The second and third plots are around low tide and show weak currents. The fourth, fifth, and sixth plots progress through the flood. Currents in the subtidal channel are oriented in the flood direction and steadily increase in magnitude through time. There is very dense spatial coverage in the main channel that extends to about the 300-m range. Coverage over the marsh is again sporadic in time and greatly reduced spatially.

b. Radar coverage statistics

As depicted in the above figures, area coverage can vary considerably during the experiment. Since the flow speed is too low to generate turbulence motion that can produce a significant surface roughness signature, the presence of 0.5-m resonant Bragg waves is dependent on the wind, as is the case with coastal ocean radar systems. Figure 5 shows the number of radial vector solutions in each 15-min data segment versus the wind speed measured at the end of the boardwalk. The figure shows that the number of vectors, which is a good measure of the area covered by the radar system, is roughly proportional to the wind speed up to approximately 4.5 m s^{-1} and is nearly independent of wind speed above 4.5 m s^{-1}.

c. Comparison with in situ velocity measurements

We deployed only a single radar, so it is not possible to resolve the total surface current velocity vector. Fortunately, the axis of the portion of the subtidal channel east of the radar is parallel to the radial vectors. At this location, the radial component derived from the radar is a good measure of the total velocity. The aquadopp was deployed in this section of the channel on 30 November and recovered on 6 December. Time series of radar-derived and measured current are depicted in Fig. 6. The aquadopp current vector is rotated (60°T) into the radial axis coordinate of the antenna so that a direct comparison between speeds is possible. The com-

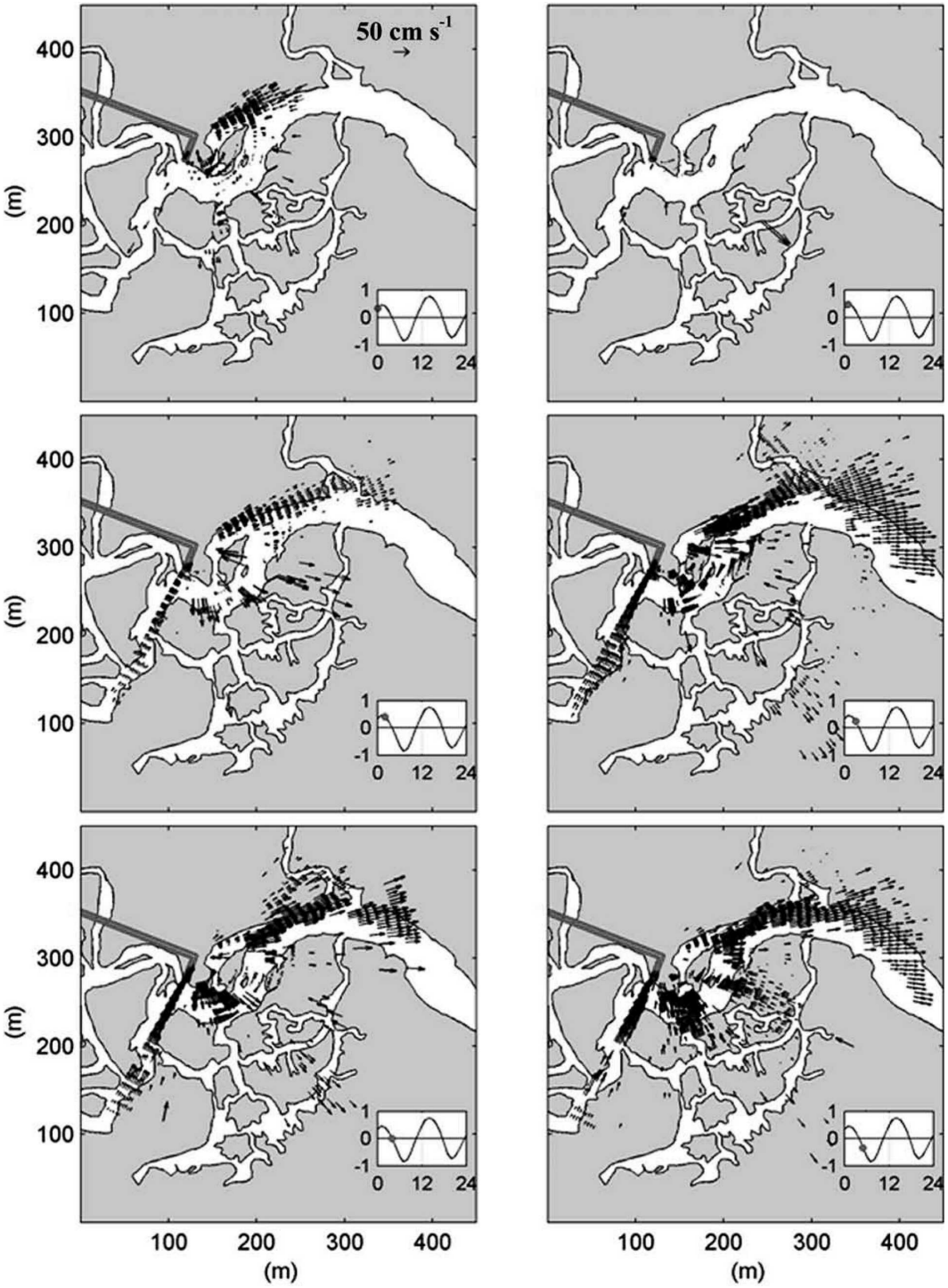

FIG. 3. RiverSonde coverage over an ebb cycle. The vector maps progress through time from left to right, top to bottom. The first map is just before high tide and each map represents hourly snapshots of the vector field. The thick solid black line denotes the boardwalk, and the creeks and channels are white. The marsh platform is gray. The inset denotes sea surface elevation (m) as a function of time (h) beginning on 16 Dec. The solid circle marks the tidal stage associated with the corresponding vector map.

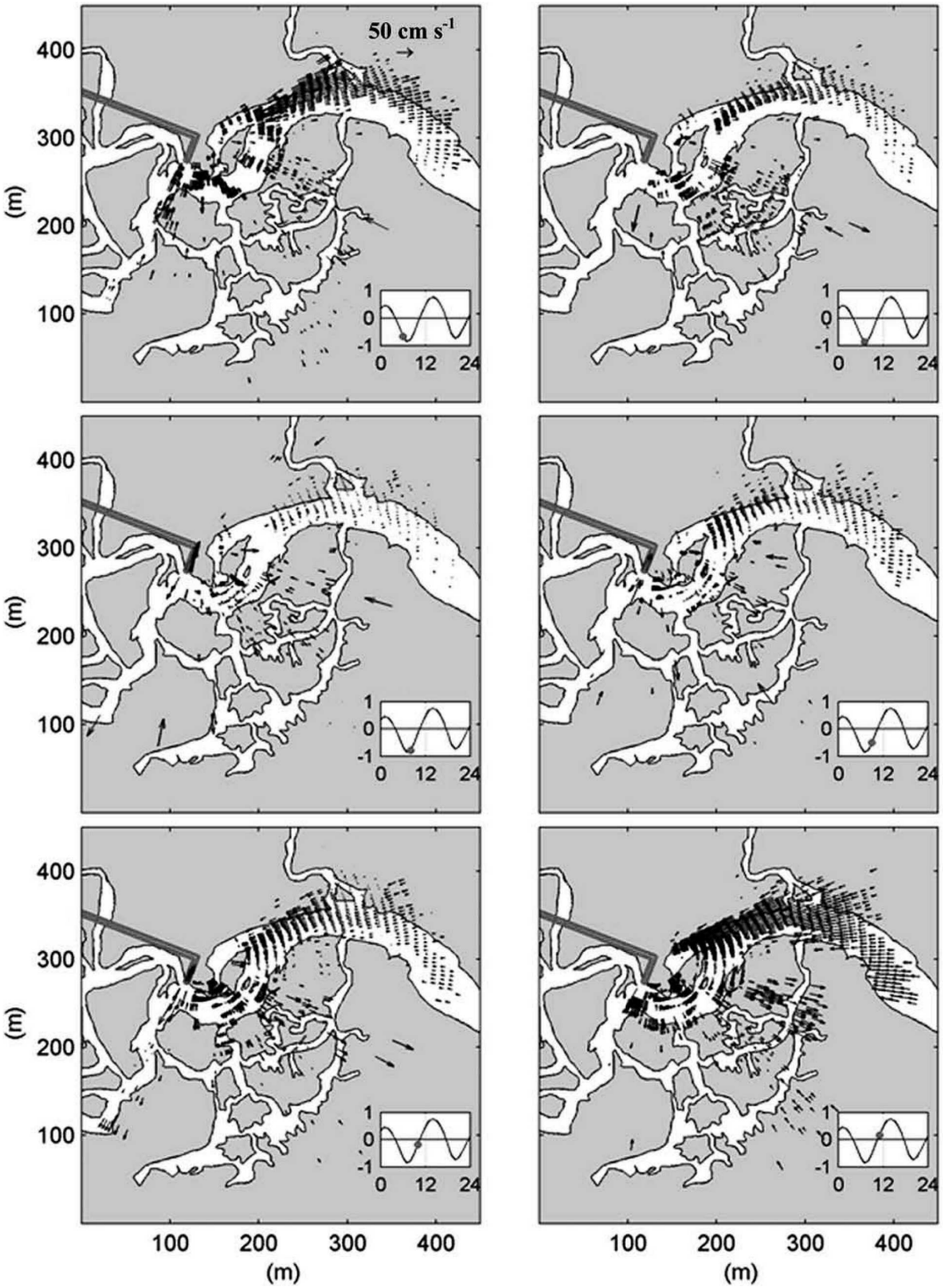

FIG. 4. Similar to Fig. 3, but for the remaining portion of the tidal cycle.

parison between the radar and the profiler is very good for most of the time period. For this 1-week period, the radar is operational 90% of the time and the wind speed is always greater than 2 m s^{-1}. The radar appears to have the proper phasing and captures the semidiurnal fluctuations in the tidal currents. Some small perturbations in the shape of the velocity curve appear at the same point in each cycle, particularly during the flood. These appear in both the radar and the aquadopp measurements, indicating that the radar is able

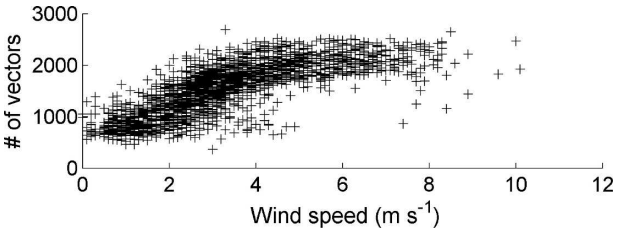

FIG. 5. Scatterplot depicting the number of radial vector solutions in each 15-min segment as a function of wind speed.

to accurately measure surface currents in marsh channels.

Figure 7 is a scatterplot depicting the difference between the aquadopp and the radar currents (residual) as a function of wind speed. The standard deviation of the residual is 0.19 m s^{-1}. Similar standard deviations have been reported for radars deployed along the central California coast (Emery et al. 2004). Significant scatter is seen for wind speeds less than about 2.5 m s^{-1}, which probably indicates that the wind is too weak to consistently generate the Bragg resonate waves required to produce a strong enough echo. At wind speeds greater than about 5 m s^{-1}, the residual tends to be negatively biased. At these wind speeds, the wind stress can generate a highly sheared surface layer such that a profiler measuring at 0.5 m below the surface may not capture the strong surface current that is measured by the radar. This effect should increase with increasing wind speed, which appears to be the case for our comparison. Similar deviations under high winds have been noted in other applications of the RiverSonde (Teague et al. 2005).

4. Discussion and conclusions

The RiverSonde is designed to be used along the side of a relatively straight, uniformly wide river channel (Teague et al. 2003), so the sinuous channels of the marsh location normally are not expected. Neverthe-

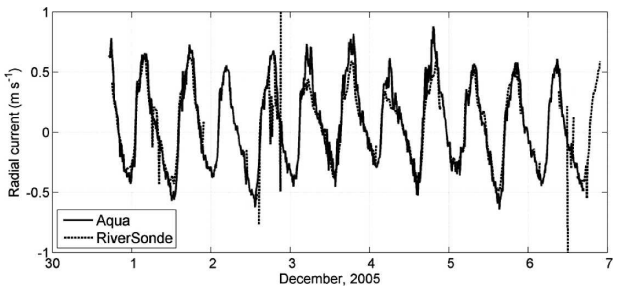

FIG. 6. Comparison between radar and aquadopp currents during the first week in December.

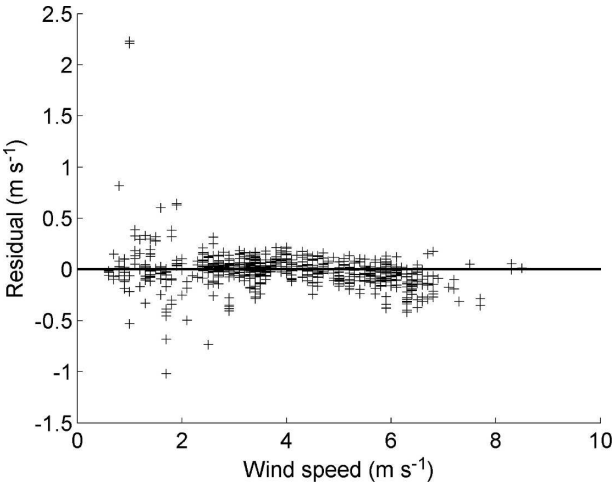

FIG. 7. Residual current (difference between the profiler and the radar) as a function of wind speed computed from the data presented in Fig. 6.

less, the system performed quite well as long as there was sufficient wind (>2 m s^{-1}) to generate the Bragg resonant waves that are required to obtain radar echoes. Our analysis of nearly 2 yr of wind speed measurements at Oyster Landing indicated that the wind speed is greater than 2 m s^{-1} 72% of the time. Assuming this wind speed is sufficient to generate the required waves provides a measure of the expected long-term performance that is possible in salt marshes. The area of the exposed water varied during the tidal cycle, as did the areal coverage of the radar system. It does not appear that the shallow water depth was a problem (the 0.5-m wavelength waves are in "deep" water if the depth is on the order of 0.25 wavelength, or about 0.12 m). Furthermore, the comparison between the measured and radar currents, which assumes a linear deep-water phase speed, indicates that linear wave theory is a good approximation to describe these small wind-generated waves. In other words, wave–current interaction effects, which are nonlinear and would complicate the theory, appear to be negligible in the channel.

One problem that was not anticipated was the energy near zero Doppler shift between the Bragg lines. It was not always seen and appeared to be correlated with the wind speed. The marsh was filled with narrow stalks of *Spartina alterniflora*, exposed about a meter above the mean water level, which probably provided effective radar targets for the vertically polarized signal. If the wind was low, their energy would be seen very close to zero Doppler shift, but if the wind increased, their energy would be spread away from dc and would approach the position of the Bragg lines. This effect can be seen in the two spectra of Fig. 2. Data for the lower

curve were obtained with a wind speed of 3.7 m s^{-1} and a water elevation of 0.98 m, while data for the upper curve were obtained with a wind speed of 10.1 m s^{-1} and a water elevation of 1.07 m, so the height of the exposed grass should be similar for the two cases. The noise floor around the Bragg lines is 10–15 dB higher for the higher wind speed. Fortunately, the motion was random, and the signals were not well correlated between the individual data segments within each 15-min window, so the simple procedure of filtering based on individual vector standard deviation and on the number of vectors was quite effective at removing those signals.

Spatial and temporal coverage in the channel was quite good, but less so over the marsh platform. Although not shown, time series measurements from cells located over the marsh surface were sporadic and fluctuated widely in magnitude between adjacent 15-min bursts. Currents on the marsh platform at North Inlet are generally on the order of a few centimeters per second or less (Torres and Styles 2007). Our preliminary findings indicate that these values are near the minimum velocity that can be reliably resolved by the radar, particularly since the marsh is only flooded around high tide when currents are near their absolute minimum. In addition, the propagation of the small surface waves required to provide suitable echo over the marsh platform in dense *Spartina* coverage is not well understood. These processes must be addressed in combination with radar applications in environments with low flow and emergent vegetation. It is likely that during strong winds accompanied by a high spring tide, when the *Spartina* is submerged, detailed spatial measurements of over marsh currents are possible with this system.

Acknowledgments. The authors extend their gratitude to the staff of the Belle W. Baruch Institute for Marine and Coastal Science for use of the facilities and logistical support in the field. We would also like to thank Hannuman Bull, Steven Traynum, and Megan Schuler for help with the current meter deployment and data analysis. Pete Lilleboe and Chad Whelan from CODAR helped set up the equipment and monitor its operation. This project was funded by the Cooperative Institute for Coastal and Estuarine Environmental Technology (CICEET) under NOAA Grant NA04NOS4190109. Partial support to RS was also provided by the SouthEast U.S. Atlantic Coastal Ocean Observation System (SEACOOS) under ONR Grant N00014-02-1-0972.

REFERENCES

Barrick, D. E., M. W. Evans, and B. L. Weber, 1977: Ocean surface currents mapped by radar. *Science,* **198,** 138–144.

Costa, J. E., K. R. Spicer, R. T. Cheng, F. P. Haeni, N. B. Melcher, E. M. Thurman, W. J. Plant, and W. C. Keller, 2000: Measuring stream discharge by non-contact methods—A proof-of-concept experiment. *Geophys. Res. Lett.,* **27,** 553–556.

——, and Coauthors, 2006: Use of radars to monitor stream discharge by noncontact methods. *Water Resour. Res.,* **42,** W07422, doi:10.1029/2005WR004430.

Emery, B. M., L. Washburn, and J. A. Harlan, 2004: Evaluating radial current measurements from CODAR high-frequency radars with moored current meters. *J. Atmos. Oceanic Technol.,* **21,** 1259–1271.

Leonard, L. A., and M. E. Luther, 1995: Flow hydrodynamics in tidal marsh canopies. *Limnol. Oceanogr.,* **40,** 1474–1484.

Melcher, N. B., and Coauthors, 2002: River discharge measurements by using helicopter-mounted radar. *Geophys. Res. Lett.,* **29,** 2084, doi:10.1029/2002GL015525.

Plant, W. J., W. C. Keller, K. Hayes, and K. Spicer, 2005: Streamflow properties from time series of surface velocity and stage. *J. Hydraul. Eng.,* **131,** 657–664.

Schmidt, R. O., 1986: Multiple emitter location and signal parameter estimation. *IEEE Trans. Antennas Propag.,* **34,** 276–280.

Spain, P., D. E. Barrick, and C. C. Teague, 2006: Remote sampling of river discharge using radar and sonar: Combining RiverSonde radar and Channel Master ADCP provides a new angle to an old measurement problem. *Sea Technol.,* **47,** 35–44.

Teague, C. C., D. E. Barrick, P. M. Lilleboe, and R. T. Cheng, 2001: Canal and river tests of a RiverSonde streamflow measurement system. *Proc. Int. Geoscience and Remote Sensing Symp.,* Sydney, Australia, IEEE, 1288–1290.

——, ——, ——, and ——, 2003: Initial river test of a monostatic RiverSonde streamflow measurement system. *Proc. Seventh Working Conf. on Current Measurement Technology,* New York, NY, IEEE/OES, 46–50.

——, ——, ——, ——, and C. A. Ruhl, 2005: UHF RiverSonde observations of water surface velocity at Threemile Slough, California. *Proc. Int. Geoscience and Remote Sensing Symp.,* Seoul, South Korea, IEEE, 4383–4386.

Torres, R., and R. Styles, 2007: Effects of topographic structure on salt marsh currents. *J. Geophys. Res.,* **112,** F02023, doi:10.1029/2006JF000508.

Traynum, S., and R. Styles, 2007: Flow, stress and sediment resuspension in a shallow tidal channel. *Estuaries Coasts,* **30,** 1–8.

Voulgaris, G., and S. T. Myers, 2004: Temporal variability of hydrodynamics, sediment concentration and sediment settling velocity in a tidal creek. *Cont. Shelf Res.,* **24,** 1659–1683.